LETTER

doi:10.1038/nature09717

A candidate redshift $z \approx 10$ galaxy and rapid changes in that population at an age of 500 Myr

R. J. Bouwens[1,2], G. D. Illingworth[1], I. Labbe[3], P. A. Oesch[4], M. Trenti[5], C. M. Carollo[4], P. G. van Dokkum[6], M. Franx[2], M. Stiavelli[7], V. González[1], D. Magee[1] & L. Bradley[7]

Searches for very-high-redshift galaxies over the past decade have yielded a large sample of more than 6,000 galaxies existing just 900–2,000 million years (Myr) after the Big Bang (redshifts $6 > z > 3$; ref. 1). The Hubble Ultra Deep Field (HUDF09) data[2,3] have yielded the first reliable detections of $z \approx 8$ galaxies[3–9] that, together with reports of a γ-ray burst at $z \approx 8.2$ (refs 10, 11), constitute the earliest objects reliably reported to date. Observations of $z \approx 7$–8 galaxies suggest substantial star formation at $z > 9$–10 (refs 12, 13). Here we use the full two-year HUDF09 data to conduct an ultra-deep search for $z \approx 10$ galaxies in the heart of the reionization epoch, only 500 Myr after the Big Bang. Not only do we find one possible $z \approx 10$ galaxy candidate, but we show that, regardless of source detections, the star formation rate density is much smaller (~10%) at this time than it is just ~200 Myr later at $z \approx 8$. This demonstrates how rapid galaxy build-up was at $z \approx 10$, as galaxies increased in both luminosity density and volume density from $z \approx 10$ to $z \approx 8$. The 100–200 Myr before $z \approx 10$ is clearly a crucial phase in the assembly of the earliest galaxies.

The detection of galaxies at very high redshift from deep imaging data depends on the absorption (by intervening neutral hydrogen) of much of the flux in the spectrum at wavelengths below the wavelength of Lyman α (121.6 nm). These 'spectral breaks' shift to longer wavelengths for more distant, redshifted galaxies seen at earlier times. A distinguishing characteristic of $z \approx 10$ galaxies would be, first, a detection in the H_{160} band, and, second, the absence of flux in the J_{125} band, and in all other shorter-wavelength Hubble Space Telescope (HST) Wide Field Camera 3 (WFC3/IR) and Advanced Camera for Surveys (ACS) filters blueward of the J_{125} band (hence they are called 'J_{125}-dropouts'). The new, powerful HST WFC3/IR camera is ~40 times more efficient at finding $z \approx 7$ galaxies[2,4–9] than the previous near-infrared NICMOS camera owing to its wider field of view and greater sensitivity in its Y_{105}, J_{125} and H_{160} filters. It provides us with the capability to explore to $z \approx 10$.

A thorough search of the deep WFC3/IR HUDF09 data set strong limits at $z \approx 10$, and also resulted in the detection of a candidate $z \approx 10$ J_{125}-dropout galaxy UDFj-39546284 at 5.4σ in our 0.26″-diameter selection aperture (Fig. 1). The signal-to-noise ratio grows to 5.8σ in a larger 0.35″-diameter aperture. The candidate is 28.92 ± 0.18 mag in the WFC3/IR H_{160} band ($(1.01 \pm 0.18) \times 10^{-31}$ erg s^{-1} cm^{-2} Hz^{-1}), has a likely redshift of $z \approx 10.3$ (Fig. 2), and appears to be slightly extended. Given the importance of the limits that we set, and of the candidate $z \approx 10$ galaxy, we perform extensive tests and simulations.

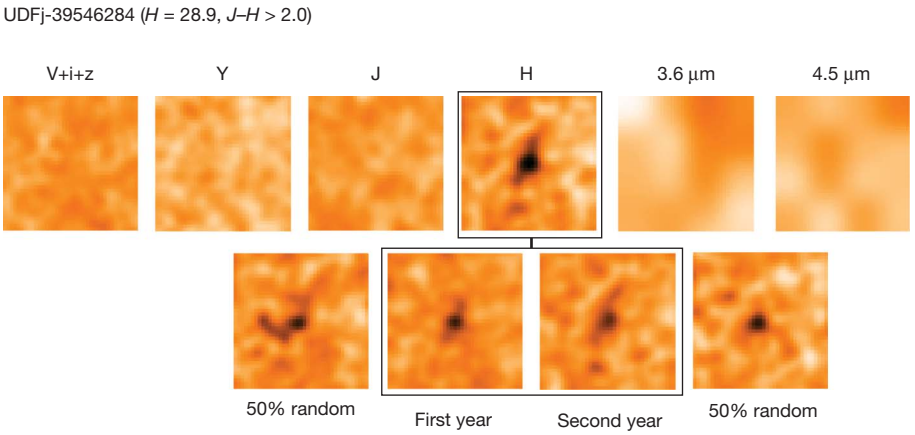

Figure 1 | Optical and near-infrared images of the candidate $z \approx 10$ galaxy, UDFj-39546284, from the HUDF. Top row: the leftmost panel shows the HUDF ACS ($V_{606}+i_{775}+z_{850}$) data[26]; the next three panels show the similarly deep HUDF09 (HST GO 11563), near-infrared WFC3/IR (Y_{105}, J_{125}, H_{160}) data (reaching to 5σ depths of ~29.8 AB mag)[2,3,9]; and the last two panels show the longer wavelength Spitzer IRAC 3.6 and 4.5 μm observations. Bottom row: the two middle panels show images of our $z \approx 10$ candidate in the first and second year of H_{160}-band observations (each representing ~50% of the total); the two outer panels show two random 50% subsets of the data (see also Supplementary Fig. 2). Each cutout is 2.4″ × 2.4″ on a side, and is orientated with north at the top. For our selection criteria, we require our $z \approx 10$ candidates to be detected at 5σ in the H_{160} band, to have $J_{125} - H_{160}$ colours redder than 1.2 AB mag, and to be undetected ($<2\sigma$) in all imaging observations blueward of the J_{125} band. Also, candidates must not be detected at $>1.5\sigma$ in more than one band blueward of the J_{125} band, and have $\chi^2 < 2.5$ in the extremely-deep image obtained by combining the B_{435}, V_{606}, i_{775}, z_{850} and Y_{105} imaging data. All of these requirements place very strong limits on the optical flux from our $z \approx 10$ candidates and provide strong discrimination against contamination by low-redshift sources (see ref. 9, Appendix C). The candidate is significant at $>3\sigma$ in each year of observations and therefore not likely to be spurious. It is detected at 5.4σ in the H_{160} band, which is much more significant than the next possible candidates (seen at 4.0σ and 4.9σ). In addition, our $z \approx 10$ candidate is not detected in the IRAC data, as expected given the IRAC flux limits. The position and other properties of this candidate are given in Supplementary Table 1.

[1]Department of Astronomy, University of California Santa Cruz, Santa Cruz, California 95064, USA. [2]Leiden Observatory, Leiden University, Leiden NL-2333, The Netherlands. [3]Carnegie Observatories, Pasadena, California 91101, USA. [4]Institute for Astronomy, ETH Zurich, Zurich CH-8093, Switzerland. [5]University of Colorado, Center for Astrophysics and Space Astronomy, Boulder, Colorado 80303, USA. [6]Department of Astronomy, Yale University, New Haven, Connecticut 06520, USA. [7]Space Telescope Science Institute, Baltimore, Maryland 21218, USA.

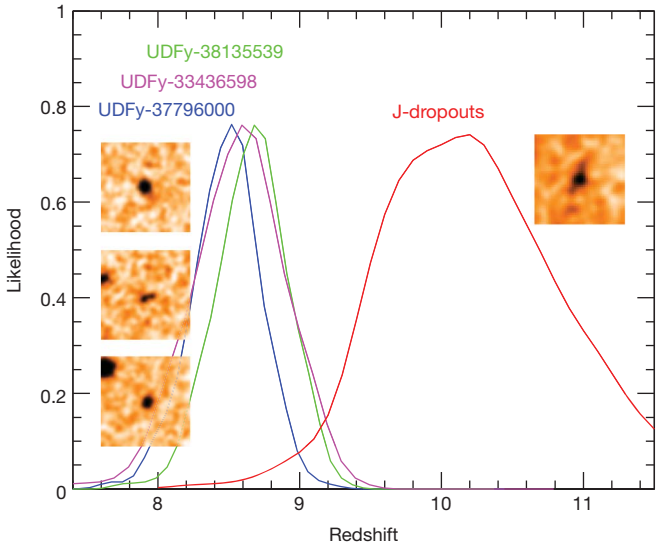

Figure 2 | Predicted redshift distributions for our $z \approx 8.5$ and $z \approx 10$ galaxy candidates. The red line gives the redshift distribution for our $z \approx 10$ J_{125}-dropout candidate, while the blue, green and magenta lines give the redshift distributions for our $z \approx 8.5$ Y_{105}-dropout candidates. The H_{160}-band source images that correspond to the redshift distributions are shown for the $z \approx 8.7$, 8.6 and $z \approx 8.5$ sources (labels arranged in same order as images), and for our $z \approx 10.3$ candidate. Each source image is $2.4'' \times 2.4''$, with north at the top. The selection criteria for the $z \approx 8$–9 sources have been published elsewhere[3,9] (see also Supplementary Information section 5). However, the detailed redshift distributions are shown here for the first time. The redshift distributions were derived by adding artificial sources to the HUDF09 WFC3/IR data, and re-selecting them in the same way as the actual galaxy candidates (see Supplementary Information sections 4, 5 and 9). The mean redshifts of these distributions are 8.7, 8.6, 8.5 and 10.3. The $z \approx 8.7$ source has a tentative spectroscopic confirmation at $z \approx 8.6$ (ref. 14). For these simulations, the ultraviolet luminosity function was used. The luminosity function describes the number density of galaxies versus luminosity and is usually parameterized as $\phi^* e^{-L/L^*}(L/L^*)^{\alpha}$, where ϕ^* is the normalization, L^* is the characteristic luminosity, and α is the faint end slope (see Fig. 3). The luminosity function was assumed to have an M^*_{UV} of -19.5 and -18.8 at $z \approx 8$ and $z \approx 10$, respectively (based on predictions from our $z \approx 4$–6 fitting relation[9,22]), while α was taken to be -1.74.

These are described in Supplementary Information sections 4 and 7, while the candidate properties are given in Supplementary Table 1.

The existence of galaxies at $z > 8.2$ (the γ-ray burst redshift[10,11]) is strengthened by three additional sources that have been detected in recent searches[3–9], one of which has a tentative spectroscopic confirmation at $z = 8.6$ (ref. 14). The updated redshift distributions from our simulations show that these three sources[3] are most likely to be at $z \approx 8.7$, 8.5 and 8.6 (Fig. 2). The expectation of finding galaxies at $z \approx 10$, just ~120 Myr earlier, is enhanced by these strong detections at $z \approx 8.5$, especially since the $z \approx 7$–8 Spitzer and HST data suggest that substantial star formation is likely at $z > 9$–10 (refs 12, 13).

The photometric-selection 'dropout' approach has been verified through numerous spectroscopic confirmations at redshifts from $z \approx 2$ to $z \approx 6$ (refs 15–19), and possibly also now at $z \approx 8.6$ (ref. 14). For our candidate $z \approx 10$ galaxy, however, its single band (H_{160} band) detection increases the risk of contamination compared to the $z \approx 7$ and $z \approx 8$ samples, where two (or more) bands are used to measure the source magnitudes and colours. Fortunately, we can test the robustness of the single-band detection process by selecting $z \approx 8$ galaxy candidates using the J_{125}-band data alone. Analogous to the $z \approx 10$ J_{125}-dropouts, $z \approx 8$ galaxies are Y_{105}-band dropouts. We compare this single-band selection against the more robust $z \approx 8$ detections using two bands[3] (J_{125} and H_{160}). We are very encouraged that we select the same eight $z \approx 8$ Y_{105}-dropouts with the J_{125}-band data alone, as we do with the normal selection using both the J_{125}- and H_{160}-band data. The primary reason for the robustness is the non-detection in all shorter wavelength filters. The χ^2_{opt} test that we have developed[9] largely eliminates contaminating objects.

Our $z \approx 10$ candidate was also checked for any Spitzer IRAC flux in the 3.6 μm band (see Fig. 1). It is quite isolated and is not detected to ~27 AB mag (2σ), further enhancing the case that this $z \approx 10$ candidate corresponds to a very-high-redshift galaxy rather than a highly reddened, lower-redshift contaminant. Contamination from spurious sources is also an important concern for such faint sources. We verified that the source is present in a wide variety of subsets of the H_{160}-band data (Fig. 1, Supplementary Fig. 2), suggesting that the candidate is not spurious. Although these tests make a case for this source being a $z \approx 10$ galaxy, deeper observations—involving both imaging (with, for example, WFC3/IR) and spectroscopy (with the James Webb Space Telescope)—will be required to confirm it.

Using the results of these tests and Monte Carlo simulations, we estimate there is an ~20% probability that our candidate is a contaminant or is spurious. Of that 20%, 10% was estimated to be from photometric scatter. Contamination from spurious sources is uncertain, and our estimates range from 1% to 10% probability; to be conservative we adopt 10%. Contamination from lower-redshift red sources is also possible, but the above single-filter $z \approx 8$ Y_{105}-dropout test suggests that the probable contamination is small, consistent with the totals we estimate from our other tests (~20%).

Fortunately, the depth of the data and the thoroughness of our analysis for contamination allow us to set very strong constraints on the volume density of $z \approx 10$ galaxies, regardless of the uncertainties associated with our candidate $z \approx 10$ galaxy. Thus we evaluate our constraints based on the limit set if no galaxies were found, and based on the candidate $z \approx 10$ galaxy, whose volume density is corrected by 20% to account for the estimated contamination rate.

Large-scale structure uncertainties are important for small area searches. We estimate the field-to-field variance on the present $z \approx 10$ J_{125}-dropout searches in the HUDF09 field to be 39% (see Supplementary Information)[20]. Even at this level, the cosmic variance ('large-scale structure') is not the dominant source of uncertainty for our single candidate galaxy.

These $z \approx 10$ results have far-reaching implications for estimating the role of galaxies in reionization (using the luminosity density), and for establishing the star formation rate density at very early times, as $z \approx 10$ is just 480 Myr after the Big Bang and just a few hundred million years since the first galaxies formed. Strikingly, the upper limits and our candidate allow us to do this through quantitative constraints we place on the $z \approx 10$ luminosity function.

The extent of the changes at $z \approx 10$ can be demonstrated by first contrasting what we see at $z \approx 10$ with expectations based on a 'no-evolution' scenario: that is, the galaxy populations stay unchanged with time. We compute the 'no-evolution' estimate by using our 'galaxy cloning' software[21] to artificially redshift the observed $z \approx 6$ and $z \approx 7$ galaxy population to $z \approx 10$, add them at random positions within our HUDF data, and then repeat the object selection process just as for the observed $z \approx 10$ galaxies. We estimated that we would find 12 ± 4 $z \approx 10$ galaxies using our $z \approx 7$ detections as the baseline, and 23 ± 5 $z \approx 10$ galaxies using our $z \approx 6$ detections as a baseline. These 'no-evolution' estimates are substantially higher than our (contamination-corrected) estimate of ~0.8 $z \approx 10$ galaxies. For simple Poissonian statistics, our observed number of ~0.8 galaxies is inconsistent with no-evolution at 4σ and 5σ confidence, respectively (and sets even stronger limits on any 'upturn' in the star formation rate[6]). Although striking, this is not wholly unexpected. Extrapolating the trends seen by us at lower redshifts[22] would lead us to expect 3 ± 2 $z \approx 10$ sources. Thus our results reaffirm that the significant evolution seen in galaxies at lower redshift continues to $z \approx 10$ (in contrast with other studies[6]).

The present search results can also be expressed as constraints on the luminosity function at $z \approx 10$. The luminosity function describes

the number density of galaxies versus luminosity, and is important for estimating the ultraviolet flux from galaxies and their expected role in reionizing the Universe. The high-redshift-galaxy ultraviolet luminosity function maintains a nearly constant form and evolves in a largely self-similar manner, with the characteristic luminosity (L^*) increasing smoothly over about 1,300 Myr from $z \approx 7$ to $z \approx 3$, that is, from ~750 Myr to ~2,000 Myr. Assuming the same form for the ultraviolet luminosity function at $z \approx 10$, we find that L^* at $z \approx 10$ is fainter, indicating that the evolution in the bright end of the ultraviolet luminosity function seen from $z \approx 7$ to $z \approx 4$ (refs 1, 9, 22) continues to $z \approx 10$ (Fig. 3). Definitive measurements of L^* at $z \approx 10$ will, of course, require deep, wide-area data to define the luminous end of the $z \approx 10$ luminosity function.

The existence of a steep slope α to the faint end of the ultraviolet luminosity function found at $z \approx 6$–7 (refs 1, 2, 9) highlights the importance of low luminosity galaxies in providing the flux needed to reionize the Universe. It is of great interest to estimate the ultraviolet luminosity density at $z \approx 7$–10 where reionization most probably occurred, given its apparent completion at $z \approx 6$ (ref. 23) and its onset at $z \approx 11$ as deduced from Wilkinson Microwave Anisotropy Probe (WMAP)[24] observations. The recent results from the HUDF09 data set provide estimates for the ultraviolet luminosity density at $z \approx 7$ and at $z \approx 8$ (ref. 9). We can now also do so at $z \approx 10$. We compute the luminosity density implied by our sample by assuming a faint-end slope of −1.7 (the same slope as found for the $z \approx 2$–7 luminosity functions) and extending the integration down to a very plausible limit of −12 AB mag. We find that the ultraviolet flux that is available from

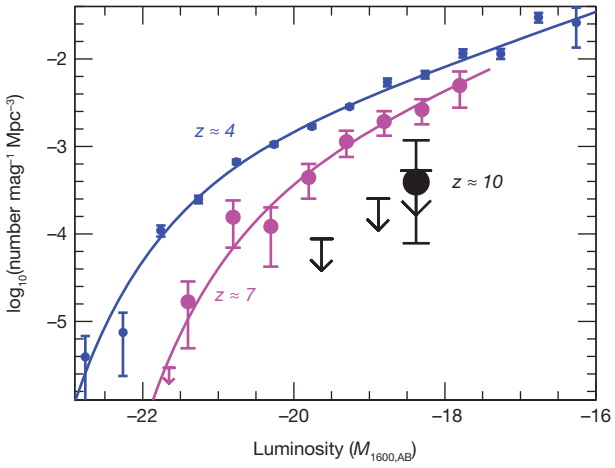

Figure 3 | Ultraviolet luminosity functions at $z \approx 4$, $z \approx 7$ and constraints for $z \approx 10$. The present constraints on the stepwise ultraviolet luminosity function at $z \approx 10$ (black points and upper limits) are new and are derived from the J_{125}-dropout candidate galaxies over our ultra-deep HUDF WFC3/IR field. These luminosity functions are a function of the absolute magnitude (that is, luminosity) of galaxies ($M_{1600,AB}$) in the rest-frame far-ultraviolet. All error bars are 1σ. The stepwise luminosity function at $z \approx 10$ is also presented as a 1σ upper limit, given the uncertainty of our $z \approx 10$ candidate. The lowest luminosity point has been corrected for incompleteness. The ultraviolet luminosity functions[1,9] at $z \approx 4$ (blue) and at $z \approx 7$ (magenta) are shown for comparison. The luminosity functions fitted here are of the form $\phi^* e^{-L/L^*}(L/L^*)^{\alpha}$ (see Fig. 2 legend). This analytic representation has recently been shown[9] to fit well at $z \approx 7$ and later times. The present search results also allow us to estimate the value of L^* at $z \approx 10$—assuming that the luminosity function at $z \approx 10$ has the same values of ϕ^* and $\alpha \approx -1.7$ as have been found to describe ultraviolet luminosity function results from $z \approx 7$ to $z \approx 4$ (refs 1, 2, 9, 27–29). Doing so allows us to constrain the evolution in the luminosity function out to $z \approx 10$, nearly 500 Myr earlier than at $z \approx 6$ (and so halving the time difference between the first galaxies at $z \approx 15$–20 and those seen at $z \approx 6$). We find L^* at $z \approx 10$ to be -18.3 ± 0.5 AB mag, or $L^* > -18.3$ in the limit of no detected sources—although obviously very uncertain, this is consistent with the evolution in the bright end of the ultraviolet luminosity function seen from $z \approx 7$ to $z \approx 4$ continuing to $z \approx 10$.

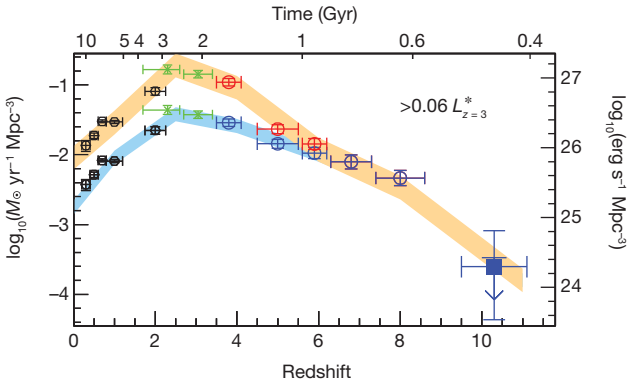

Figure 4 | The luminosity density and star formation rate density in the Universe over 13.2 Gyr. The rest-frame continuum ultraviolet luminosity density (right axis, blue points) at $z \approx 10$, and the star formation rate density (left axis, red points) derived from the extinction-corrected luminosity density[1,25], are integrated down to the approximate magnitude limit $M_{AB} \approx -18$ (0.06L^*) of our $z \approx 10$ J_{125}-dropout search. The conversion from ultraviolet luminosity to star formation rate assumes a Salpeter initial mass function. The upper horizontal axis gives the time after the Big Bang and the lower axis the redshift. As before, we assume that the ultraviolet luminosity function has the same faint-end slope (and normalization) as at $z \approx 6$ and $z \approx 7$. The star formation rate density ($1.9^{+4.4}_{-1.5} \times 10^{-4}\ M_{\odot}\ \mathrm{yr}^{-1}\ \mathrm{Mpc}^{-3}$) from the contamination-corrected sample is shown at $z \approx 10$ from the current J_{125}-dropout search, as is the 1σ upper limit ($< 3 \times 10^{-4}\ M_{\odot}\ \mathrm{yr}^{-1}\ \mathrm{Mpc}^{-3}$) if we assume no $z \approx 10$ sources are detected. All error bars are 1σ. Also included here are the recent star formation rate determinations at $z \approx 7$ and $z \approx 8$ from our HUDF09 WFC3/IR z_{850}-dropout and Y_{105}-dropout searches[9], and from the literature at $z < 4$ (green and black points: refs 27, 30) and at $z \approx 4$–6 (ref. 1). The dust corrections at $z \approx 4$ are based on the estimated ultraviolet-continuum slopes β, and are already negligible by $z \approx 7$ (refs 2, 3, 25). There is no evidence for any substantial change in the star formation rate density trends established at lower redshift.

galaxies at $z \approx 10$ is only $\sim 12^{+26}_{-10}$% of what is needed for galaxies to be the reionizing source, with typical assumptions of an escape fraction of ~0.4, a clumping factor of ~3 and a Salpeter initial mass function (see, for example, ref. 9). This result is tantalizing, suggesting that galaxies are contributing to reionization, but the enigma remains: where are most of the needed ultraviolet photons coming from? Observations to significantly fainter levels will be central to characterizing the role of galaxies in reionization.

The star formation rate (SFR) density is derived from the luminosity density (see Fig. 4). The SFR density increases systematically and monotonically at early times from $z \approx 10$ (500 Myr) to $z \approx 4$ (1,600 Myr), peaking at $z \approx 2$–3 (at ~2,500 Myr), before decreasing at $z < 2$ (Fig. 4). This suggests that the luminosity function and star formation rate density evolution found at lower redshifts[1,25] continues to $z \approx 10$ when the universe was just 480 Myr old. The limits established here even suggest that the trends in star formation rate density established at lower redshifts could be steepening.

This is clearly an era when galaxies were evolving very rapidly. The star formation rate density increased by a factor of ~10 in less than 200 Myr, from $z \approx 10$ to $z \approx 8$. This dramatic change in such a short period of time suggests that the first phases of galaxy formation and their build-up could be unveiled by observations that penetrate just 200 Myr earlier, to redshifts $z \approx 15$. However, only when the James Webb Space Telescope is launched will these first phases of galaxy build-up between $z \approx 15$ and $z \approx 10$ be revealed.

Received 21 December 2009; accepted 30 November 2010.

1. Bouwens, R. J., Illingworth, G. D., Franx, M. & Ford, H. UV luminosity functions at z~4, 5, and 6 from the Hubble Ultra Deep Field and other deep Hubble Space Telescope ACS fields: evolution and star formation history. *Astrophys. J.* **670,** 928–958 (2007).
2. Oesch, P. A. *et al.* z~7 Galaxies in the HUDF: first epoch WFC3/IR results. *Astrophys. J.* **709,** L16–L20 (2010).

3. Bouwens, R. J. *et al.* Discovery of z~8 galaxies in the HUDF from ultra-deep WFC3/IR observations. *Astrophys. J.* **709,** L133–L137 (2010).
4. McLure, R. *et al.* Galaxies at z~6–9 from the WFC3/IR imaging of the HUDF. *Mon. Not. R. Astron. Soc.* **403,** 960–983 (2010).
5. Bunker, A. *et al.* The contribution of high redshift galaxies to cosmic reionization: new results from deep WFC3 Imaging of the Hubble Ultra Deep Field. *Mon. Not. R. Astron. Soc.* **409,** 855–866 (2010).
6. Yan, H. *et al.* Galaxy formation in the reionization epoch as hinted by Wide Field Camera 3 observations of the Hubble Ultra Deep Field. *Res. Astron. Astrophys.* **10,** 867–904 (2010).
7. Finkelstein, S. *et al.* On the stellar populations and evolution of star-forming galaxies at 6.3<z8.6. *Astrophys. J.* **719,** 1250–1273 (2010).
8. Robertson, N., Ellis, R. S., Dunlop, R. S., McLure, R. J. & Stark, D. P. Early star-forming galaxies and the reionization of the Universe. *Nature* **468,** 49–55 (2010).
9. Bouwens, R. J. *et al.* UV luminosity functions from 113 z~7 and z~8 Lyman-break galaxies in the ultra-deep HUDF09 and wide-area ERS WFC3/IR observations, 2010. *Astrophys. J.* (submitted); preprint at ⟨http://arxiv.org/abs/1006.4360⟩ (2010).
10. Tanvir, N. *et al.* A γ-ray burst at a redshift of z ≈ 8. *Nature* **461,** 1254–1257 (2009).
11. Salvaterra, R. *et al.* GRB090423 at a redshift of *z* ≈ 8.1. *Nature* **461,** 1258–1260 (2009).
12. Labbé, I. *et al.* Ultradeep IRAC observations of sub-L* z~7 and z~8 galaxies in the HUDF: the contribution of low-luminosity galaxies to the stellar mass density and reionization. *Astrophys. J.* **708,** L26–L31 (2010).
13. González, V. *et al.* Stellar mass density and specific star formation rates of the Universe at z~7. *Astrophys. J.* **713,** 115–130 (2010).
14. Lehnert, M. *et al.* Spectroscopic confirmation of a galaxy at *z* = 8.6. *Nature* **467,** 940–942 (2010).
15. Steidel, C. C., Giavalisco, M., Pettini, M., Dickinson, M. & Adelberger, K. L. Spectroscopic confirmation of a population of normal star-forming galaxies at redshifts z > 3. *Astrophys. J.* **462,** L17–L21 (1996).
16. Vanzella, E. *et al.* Spectroscopic observations of Lyman break galaxies at redshifts ~4, 5, and 6 in the Goods-South Field. *Astrophys. J.* **695,** 1163–1182 (2009).
17. Popesso, P. *et al.* The great observatories origins deep survey. VLT/VIMOS spectroscopy in the GOODS-south field. *Astron. Astrophys.* **494,** 443–460 (2009).
18. Steidel, C. C. *et al.* Lyman break galaxies at redshift z ~ 3: survey description and full data set. *Astrophys. J.* **592,** 728–754 (2003).
19. Reddy, N. *et al.* A spectroscopic survey of redshift 1.4<~z<~3.0 galaxies in the GOODS-North Field: survey description, catalogs, and properties. *Astrophys. J.* **653,** 1004–1026 (2006).
20. Trenti, M. & Stiavelli, M. Cosmic variance and its effect on the luminosity function determinations in deep high-z surveys. *Astrophys. J.* **676,** 767–780 (2008).
21. Bouwens, R. J., Broadhurst, T. J. & Silk, J. Cloning Hubble Deep Fields. I. A model-independent measurement of galaxy evolution. *Astrophys. J.* **506,** 557–578 (1998).
22. Bouwens, R. J., Illingworth, G. D., Franx, M. & Ford, H. z ~ 7–10 galaxies in the HUDF and GOODS Fields: UV luminosity functions. *Astrophys. J.* **686,** 230–250 (2008).
23. Fan, X. *et al.* Evolution of the ionizing background and the epoch of reionization from the spectra of z~6 quasars. *Astron. J.* **123,** 1247–1257 (2002).
24. Komatsu, E. *et al.* Seven-Year Wilkinson Microwave Anisotropy Probe observations: cosmological interpretation. *Astrophys. J.* (in the press); preprint at ⟨http://arXiv.org/abs/1001.4538⟩ (2010).
25. Bouwens, R. *et al.* UV-continuum slope and dust obscuration from z~6 to z~2: the star formation rate density at high redshift. *Astrophys. J.* **705,** 936–961 (2009).
26. Beckwith, S. W. *et al.* The Hubble Ultra Deep Field. *Astrophys. J.* **132,** 1729–1755 (2006).
27. Reddy, N. & Steidel, C. C. A steep faint-end slope of the UV luminosity function at z ~ 2–3: implications for the global stellar mass density and star formation in low-mass halos. *Astrophys. J.* **692,** 778–803 (2009).
28. Yoshida, M. *et al.* Luminosity functions of Lyman break galaxies at z~4 and z~5 in the Subaru Deep Field. *Astrophys. J.* **653,** 988–1003 (2006).
29. McLure, R., Cirasuolo, M., Dunlop, J. S., Foucaud, S. & Almaini, O. The luminosity function, halo masses, and stellar masses of luminous Lyman-break galaxies at 5<z6. *Mon. Not. R. Astron. Soc.* **395,** 2196–2209 (2009).
30. Schiminovich, D. *et al.* The GALEX-VVDS measurement of the evolution of the far-ultraviolet luminosity density and the cosmic star formation rate. *Astrophys. J.* **619,** L47–L50 (2005).

Supplementary Information is linked to the online version of the paper at www.nature.com/nature.

Acknowledgements We are grateful to all those at NASA, STScI and throughout the community who have worked to make the Hubble Space Telescope the observatory that it is today, and we acknowledge the importance of the servicing missions and those who organised them. We acknowledge our program coordinator W. Januszewski for his care in helping to set up our program and observing configuration. We acknowledge support from NASA and the Swiss National Science Foundation.

Author Contributions R.J.B. carried out the most of the data analysis and calculations for this paper, and wrote most of the Supplementary Information; G.D.I. wrote most of the text in the Letter and iterated on the initial science results and content with R.J.B.; I.L., P.A.O., M.T., C.M.C., P.G.v.D., M.F., M.S. and L.B. provided significant feedback on the science content and on the drafts; I.L. and V.G. were involved with processing the Spitzer IRAC data; P.A.O. contributed to the data analysis; M.T. made the cosmic variance estimates; and D.M. was involved in data processing and pipeline generation for the WFC3/IR data.

Author Information Reprints and permissions information is available at www.nature.com/reprints. The authors declare no competing financial interests. Readers are welcome to comment on the online version of this article at www.nature.com/nature. Correspondence and requests for materials should be addressed to R.J.B. (bouwens@ucolick.org).